Novel self-assembled 2D networks based on zinc metal ion co-ordination: synthesis and comparative study with 3D network

ARTICLE *in* RSC ADVANCES · APRIL 2014

Impact Factor: 3.84 · DOI: 10.1039/C3RA47377E

RSC Advances

PAPER

View Article Online
View Journal | View Issue

Cite this: *RSC Adv.*, 2014, **4**, 17680

Novel self-assembled 2D networks based on zinc metal ion co-ordination: synthesis and comparative study with 3D networks†

Deepa Rajwar,[a] Xinfeng Liu,[b] Zheng Bang Lim,[a] Sung Ju Cho,[a] Shi Chen,[b] Jens M. H. Thomas,[c] Abbie Trewin,[d] Yeng Ming Lam,[a] Tze Chien Sum*[b] and Andrew C. Grimsdale*[a]

Received 6th December 2013
Accepted 28th March 2014

DOI: 10.1039/c3ra47377e

www.rsc.org/advances

The synthesis of linear and trigonal terpyridine bearing molecules (tpys) and their self-assembly to form novel extended self-assembled 2D networks of trigonal tpys with linear tpys through zinc metal ion (Zn^{2+}) co-ordination is reported. The resulting Zn^{2+} co-ordination networks have been characterized by means of X-ray photoelectron spectroscopy (XPS), small angle X-ray scattering (SAXS), BET, and photophysical methods. The presence of some short range order in these networks has been shown by the SAXS results and these results have been analyzed with the help of molecular modelling studies. These metallo-supramolecular Zn^{2+} networks revealed the influence of the metal ion on the thermal and optical properties of the synthesized metallo-supramolecular assemblies, similar to the results previously reported for 1D and 3D self-assembled metallo-supramolecular materials. Moreover, these networks have shown high luminescence with a long fluorescence lifetime and good thermal stabilities. The monolayer of such ordered networks can be used as a template to build hierarchical nanostructures. These hierarchical nanostructures could be used as active components in electronic devices and as templates for the formation of hybrid organic–inorganic nanomaterials.

Introduction

Ordered 1D, 2D and 3D structures formed through self-assembly of organic molecules by non-covalent processes such as metal–ligand co-ordination offer considerable prospects for advances in nanoscience and progress in nanotechnology. The field of supramolecular electronics has progressed rapidly in recent years.[1–4] Supramolecular electronics is one of the most promising "bottom-up" techniques in nanoelectronics of π-conjugated molecules with a device length of 5–100 nm. Supramolecular π-conjugated 'oligomers' have attracted much attention in last few decades due to the reversibility of the non-covalent interactions (hydrogen bonds, co-ordination bonds, hydrophobic interactions, electrostatic, and van der Waals interactions). Self-assembly rapidly and easily generates large and complex "supramolecules" (ensembles of individual molecules) from easily available building blocks with maximum efficiency. Synthesis of supramolecular networks from these building blocks becomes straightforward due to the thermodynamically driven self-correcting ability of non-covalent interactions. Metallo-supramolecular networks have attracted a lot of interest, not only because of the higher strength of this non-covalent interaction in comparison to other non-covalent interactions (such as hydrogen-bonding) but also for the self-healing ability and reversibility of these networks due to their dynamic nature. Co-ordination driven self-assembly, gives a better control over the rational design of supramolecular networks by taking advantage of the predictable nature of the metal–ligand co-ordination and ability of ligands to program directionality.[5,6]

Thus, this strategy of metal–ligand co-ordination represents an alternative method for "bottom-up" technique in nano-electronics by synthetic approach for designing molecules of required dimensions of few nanometers. For instance, a wide range of 1D, 2D and 3D systems formed by co-ordination bonding have been widely explored in past years.[7–12] Hence, these supramolecular co-ordination networks have found a lot of prospective to be utilized for different nanotechnological applications. For example, supramolecular co-ordination networks formed by Fe metal ion co-ordination have been

[a]*School of Materials Science and Engineering, Nanyang Technological University, Singapore. E-mail: ACGrimsdale@ntu.edu.sg; Fax: +65-6790 9081; Tel: +65-6790 6728*

[b]*Division of Physics and Applied Physics, School of Physical and Mathematical Sciences, Nanyang Technological University, Singapore. E-mail: tzechien@ntu.edu.sg; Fax: +65-6316 2971; Tel: +65-6795 7981*

[c]*Institute of Integrative Biology, University of Liverpool, Liverpool, L69 7ZB, UK*

[d]*Department of Chemistry, Lancaster University, Bailrigg, Lancaster, LA1 4YB, UK*

† Electronic supplementary information (ESI) available: NMR, CV, TGA, DSC, TEM and mass spectral data for new compounds and networks. Structures, PL profiles and PL data for S1, S3 and S4, molecular model for **1**, **3**, **N1**, and **N3**. See DOI: 10.1039/c3ra47377e

reported with excellent magnetic properties.[10] Ru^{2+} co-ordination complexes with terpyridine ligands have been used in the building of polymer wires on gold.[13] Zinc metal ion complexes are very well known for their optoelectronic properties[14–18] and are potential candidates for many optoelectronic devices. In another application, non-linear optical properties of zinc metal ion co-ordination networks have been reported recently.[19]

Terpyridines were proposed as building blocks for supramolecular chemistry decades ago.[20,21] Still there remains much scope for development in the supramolecular chemistry of terpyridines and much research work has been performed in this field.[11,13,18,22–27] Transition metal-complexes of π-conjugated bis- and tris(terpyridine) have high prospective to be used as new functional materials in electronic and optoelectronic devices. Heavy transition metal ions, such as Pt^{2+}, Ru^{2+}, Os^{2+}, and Ir^{2+} have been explored thoroughly in the past.[20,24,28] In particular, electron-poor square-planar divalent Pt^{2+} and Pd^{2+} ions have been widely used in conjunction with electron-rich nitrogen containing moieties in the self-assembly process.[25,29] Metal ions with filled electron shells have recently achieved much importance as models for the advancement of new metallopolymers. The low cost and nontoxicity of Zn^{2+} ions has made them a promising candidate for making highly developed co-ordination networks. The other advantage of using Zn^{2+} ions for co-ordination is that metal to ligand charge transfer (MLCT) processes do not occur in such systems, because of the full d10 electron configuration of the Zn^{2+} ions. Hence there is only the possibility of intraligand (IL) charge transfer in these systems. High PL quantum yields and EL performance have been reported[30] using such systems. Winter *et al.* have used Zn^{2+} as a template to assemble organic building block into polymer chains through coordination to chelating terpyridyl units.[18] These linear oligomers with tpy (2,2′:6′,2″-terpyridine) end-groups self-assembled with Zn^{2+} to give luminescent polymers. Moving one step forward towards achieving ordered and extended networks, this paper mainly focuses on the synthesis of 2D metallo-supramolecular networks of Zn^{2+} ions with terpyridine ligands and a comparison of their optoelectronic properties with the 3D networks previously reported by us.[12,19] To create metallo-supramolecular networks, monomers with

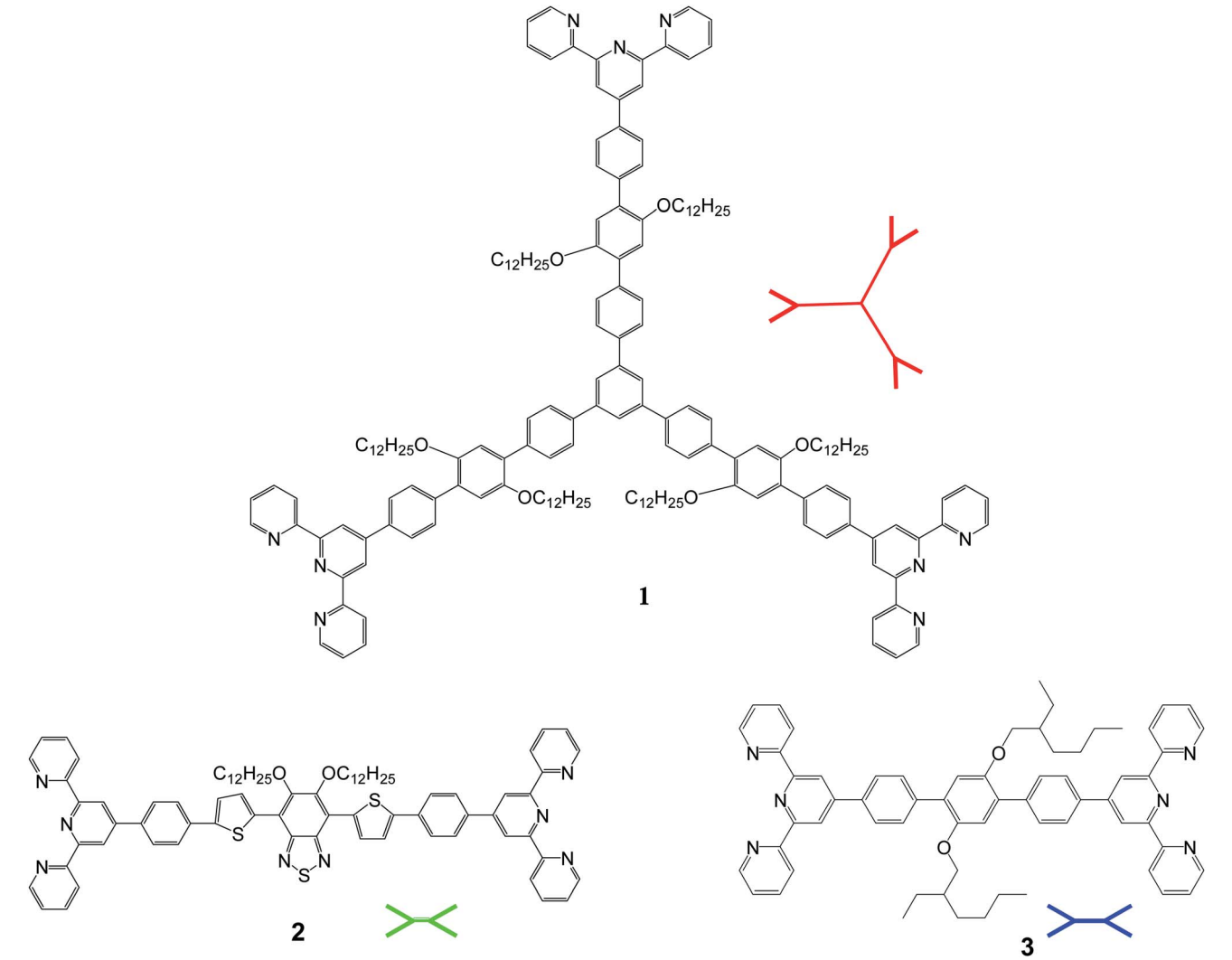

Fig. 1 Molecular structure of basic building blocks for 2D self-assembled networks.

self-assembling end-groups are mandatory. In the previous work in this field, the focus has been on linear and tetrahedral Zn^{2+} terpyridine networks. By systematic examination on their photophysical properties together with their structural characterization, it has been concluded that by changing conjugated backbone on the terpyridine units it is possible to modify the optoelectronic properties of these networks. Strong emission in the solid state indicates that these materials correspond to the capable candidates with respect to their potential applications in optoelectronic devices such as OLEDs. Hence it was anticipated that the Zn^{2+} based materials might be made solution processable by the attachment of more solubilizing groups to π-conjugated terpyridines. These complexes could be very promising candidate for solar cell applications. In extension of this work, the present investigations aim the design of zinc metal co-ordinated 2D networks made up of trigonal and linear π-conjugated terpyridines with respect to their possibility in the field of optoelectronic device applications. Various bis(terpyridine) derivatives were used in the synthesis of self-assembled supramolecular 2D networks by Zn^{2+} metal co-ordination with tpy ligands. Photophysical properties with respect to their device applications along with their thermal, and electrochemical properties, as well as ordering in their self-assembled networks, are discussed, with comparisons made to the similar 3D networks previously made by us.[12,19] The chemical structures of basic building blocks for 2D self-assembled networks are shown in Fig. 1.

Results and discussion

Synthesis

Boronation of molecule **4** through Suzuki coupling reaction gave the key intermediate core molecule **5** in a moderate yield.

Synthesis scheme of this trigonal core molecule **5** is outlined in Scheme 1. In the next step towards synthesis of molecule **1**, in the presence of Pd(0) catalyst, compound **9** was Suzuki-coupled with triborane **5** to produce compound **1** as an off white solid. The synthetic steps involved in the preparation of key intermediate molecule **9** and new 2D p-type core molecule **1** for 2D self-assembly are outlined in Schemes 2–4. The structure of this novel trigonal-tpy molecule **1** was confirmed by ^1H NMR and ^{13}C NMR and its molecular weight was confirmed by high resolution mass spectrometry (HRMS). 2D self-assembled networks of molecule **1** were made through zinc metal ion co-ordination.

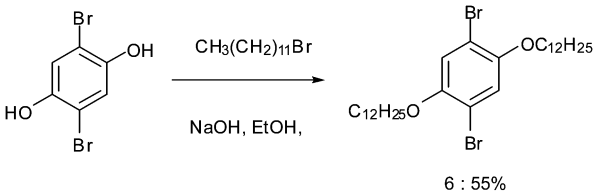

Scheme 2 Synthetic route to molecule **6**.

Formation of 2D Zn^{2+} co-ordinated self-assembled network **N1** was obtained by refluxing its 2D monomers **1** with zinc acetate ($Zn(OAc)_2$) at the stoichiometric ratio of 1 : 1.5, in NMP solutions followed by anion exchange using an excess of NH_4PF_6. Although 2D monomer **1** is soluble in common organic solvents (*e.g.* ether, DCM, $CHCl_3$, THF, *etc.*), the 2D networks **N1–3** are not only insoluble in those common organic solvents but also in highly polar aprotic solvents (*e.g.* DMSO, DMF, NMP, acetonitrile *etc.*) at room temperature. This behaviour is believed to be caused by the highly cross linked or interpenetrated structure of the 2D networks. Therefore, all the unwanted byproducts (including any unreacted starting material **1**) were washed away using ether to get the final network **N1** in solid form. The formation of new 2D Zn^{2+} co-ordinated self-assembled supramolecular network **N1** from trigonal tpy molecule **1** is shown in Scheme 5.

Using the method previously developed by us for making extended 3D networks,[12] extended networks **N2** and **N3** were formed using the p-type or n-type conjugated tpy linker units **3** and **2** as shown in Scheme 6. 2,5-Bisdodecyloxy-*p*-phenylene has been employed as the p-type linker (**3**) in **N3**. Its being linear and electron rich, it is a good electron donor. In the other extended network **N2**, 2,1,3-benzothiadiazole (benzo[*c*][1,2,5] thiadiazole) has been used as the n-type linker (**2**) as it is known to be a good electron acceptor. The same insoluble behaviour was found for the 2D extended networks **N2** and **N3**. Networks **N2** and **N3** were obtained by refluxing 2D network **N1** with zinc acetate $Zn(OAc)_2$ at the stoichiometric ratio of 1 : 1.5 in NMP solution to break the network, followed by inserting the linear

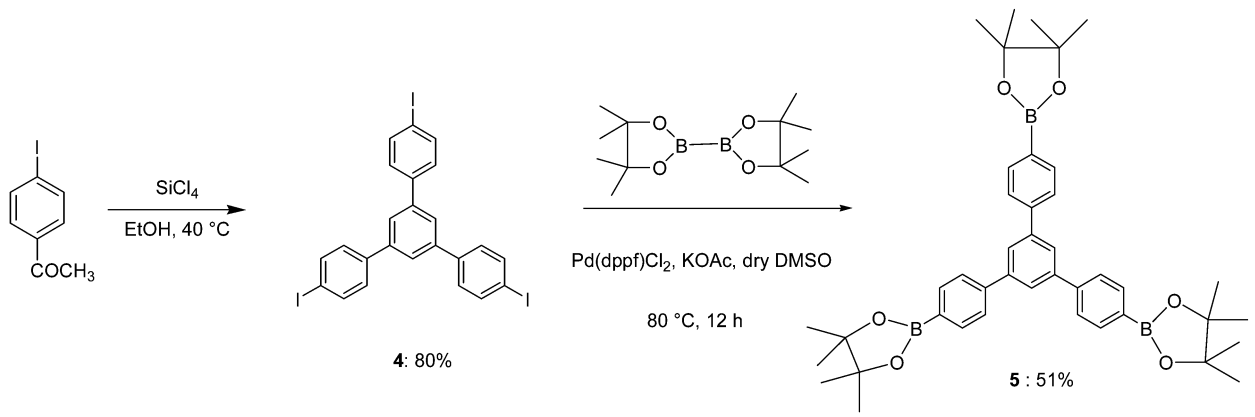

Scheme 1 Synthetic route to trigonal molecule **5**.

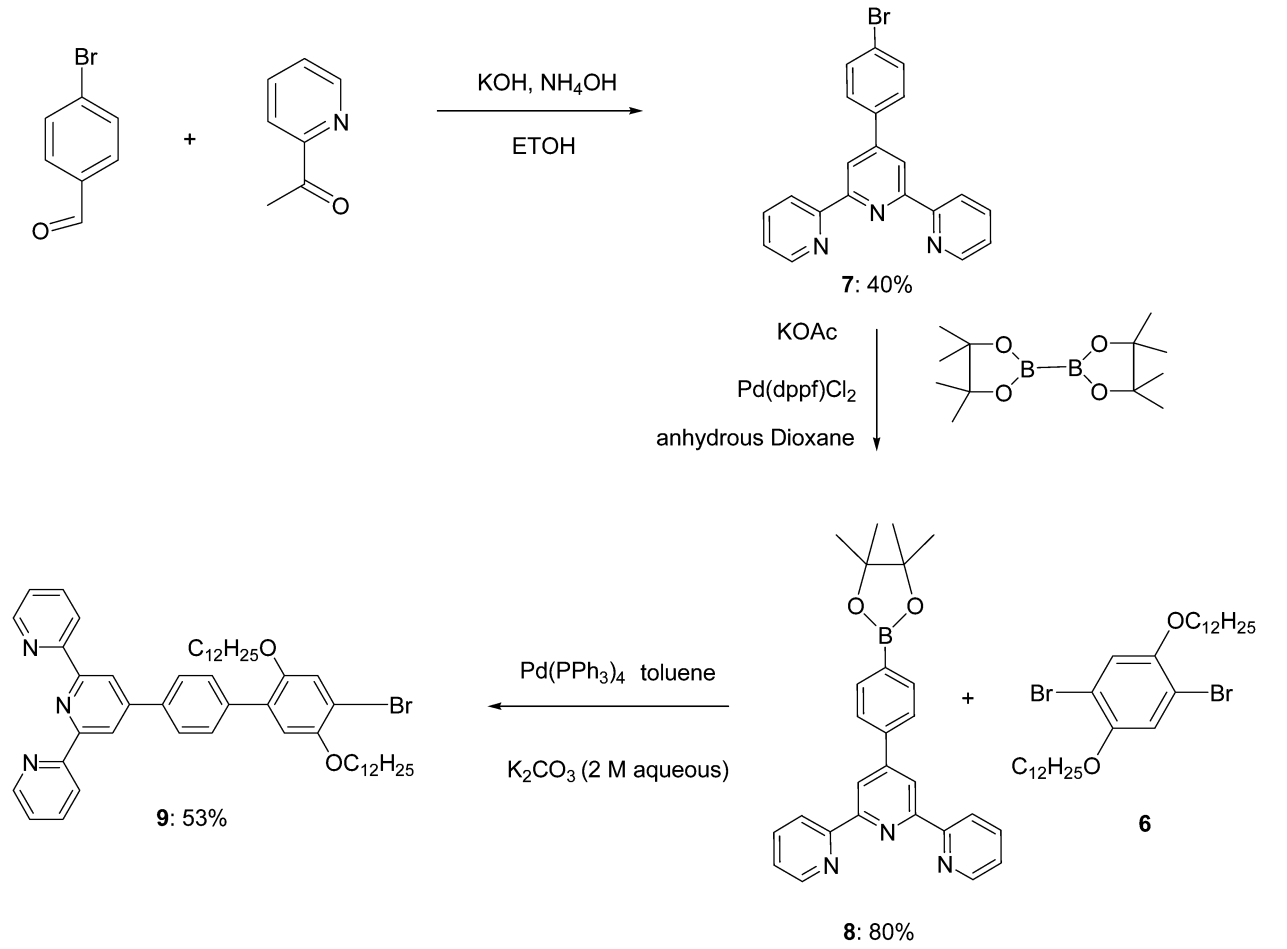

Scheme 3 Synthetic route to key intermediate molecules 7, 8 and 9.

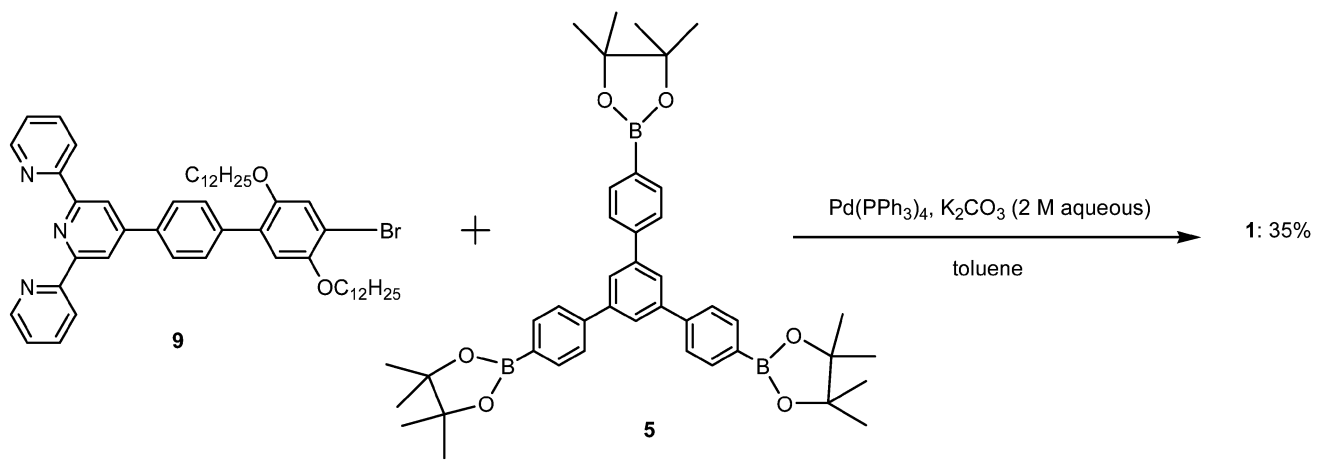

Scheme 4 Synthesis scheme of 2D supramolecule 1.

bis(tpy) monomers 2 and 3 in between the 2D molecules, respectively, to form the 2D extended networks **N2** and **N3** after anion exchange using an excess of NH_4PF_6. After forming networks **N2** and **N3**, any residual 2D starting monomer (**1**) and the linear bis(tpy) monomers (**2** and **3**) were washed away with ether.

The concept of reversible self-assembly was demonstrated in these networks which confirmed our concept for their formation. By adding more metal ions into the 2D network **N1**, co-ordination complexes can be dissociated again in favour of an open form with each zinc ion only attached to one tpy unit and its other co-ordination sites presumably saturated by solvent

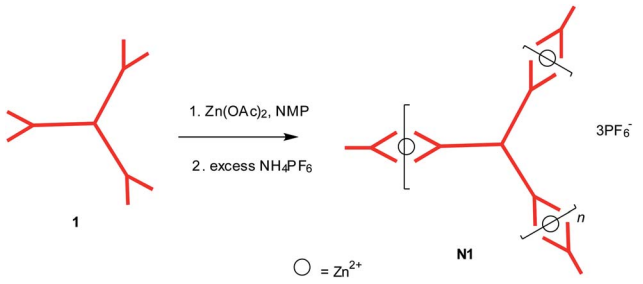

Scheme 5 Synthesis of one component 2D Zn^{2+} co-ordinated self-assembled supramolecular network **N1**.

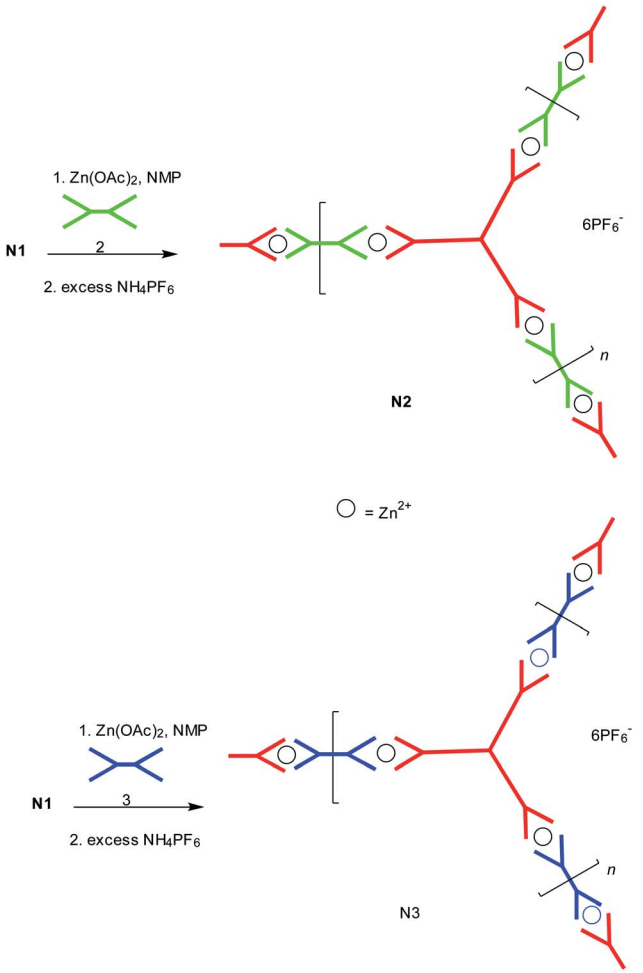

Scheme 6 Synthesis of 2D Zn^{2+} co-ordinated self-assembled two component extended supramolecular networks **N2** and **N3**.

molecules. Disassembly of **N1** was followed by re-assembly to form extended 2D networks **N2** and **N3**. 2D network **N1** was only partially soluble in the NMP solution at 105 °C and the colour of solution was light brown at that moment, after adding 1.5 equivalents of $Zn(OAc)_2$ in NMP, the insoluble solid gradually dissolved in the solution and the colour of solution gradually changed to light yellow before adding the linear bis(tpy) linkers. All these novel 2D Zn^{2+} co-ordinated self-assembled networks **N1–3** were obtained in moderate yields (>50%).

Study of presence of Zn^{2+} ion in 2D network structures

X-ray photoelectron spectroscopy (XPS) studies were performed in order to achieve an insight into the network structures. XPS measurements were performed with monochromatic Al-K alpha radiation (1486.7 eV) to confirm the existence of the zinc metal-ions and to achieve more data in favour of the proposed network structures. XPS spectra of the zinc complexes on carbon tape substrates are shown in Fig. 2. The presence of Zn 2p photo-emission peaks in **N1**, **N2** and **N3** confirms the Zn–ligand coordination. In contrast, no Zn 2p peak is present in starting material **1**. In addition, the O 1s, C 1s, N 1s and F 1s peaks (may be due to PF_6^- counterions) are also shown in widescans, indicating a successful complexation of the terpyridine units. Due to low conductivity of three networks, a few eVs charging is observed and calibrated using C 1s and other photoemission peaks. The binding energy of Zn 2p in **N1**, **N2** and **N3** located at 1020.5 eV (**N2**) and 1021.3 eV (**N1** and **N3**). The difference in binding energy could be either due to small residue charging or related to the different side chains of three networks.

Molecular organization studies of 2D network structures

Small angle X-ray scattering (SAXS) was performed to study the molecular organization. SAXS for **N1**, **N2** and **N3** in the solid state are compared. As can be seen from Fig. 3, **N1** has three clear broad peaks that centre at scattering vector $q = 0.50\ nm^{-1}$, $1.24\ nm^{-1}$ and $2.46\ nm^{-1}$ respectively. The peak at scattering vector $q = 0.50\ nm^{-1}$ ranges between 0.40 and $0.70\ nm^{-1}$. This corresponds to a distance of 12.6 nm with a range between 9.0 and 15.7 nm. The peak at scattering vector $q = 1.24\ nm^{-1}$ ranges between 1.10 and $1.50\ nm^{-1}$. This corresponds to a distance of 5.0 nm with a range between 4.0 and 5.7 nm. The peak at scattering vector $q = 2.46\ nm^{-1}$ exhibits a greater intensity and is relatively less broad than the other two peaks. It ranges between 2.00 and $3.10\ nm^{-1}$. This corresponds to a distance of 2.5 nm with a range between 2.0 and 3.1 nm.

N2 has two very broad weak peaks centred at scattering vector $q = 0.38\ nm^{-1}$ and $2.09\ nm^{-1}$ respectively. The peak at scattering vector $q = 0.38\ nm^{-1}$ ranges between 0.3 and $0.5\ nm^{-1}$. This corresponds to a distance of 1.65 nm with a range between 12.6 and 20.9 nm. The peak at scattering vector $q = 2.09\ nm^{-1}$ ranges between 1.00 and $3.10\ nm^{-1}$. This corresponds to a distance of 3.0 nm with a range between 2.0 and 6.3 nm. **N3** shows one broad but clear peak centred at scattering vector $q = 2.66\ nm^{-1}$ and ranges between 2.00 and $3.00\ nm^{-1}$. This corresponds to a distance of 2.3 nm with a range between 2.1 and 3.0 nm. **N1** shows three clear, although relatively broad, peaks compared to **N2** and **N3**, which have fewer peaks that are both weaker and broader. This suggests that **N1** has a more defined structure compared to **N2** and **N3**. This reflects the single component self-assembly composition of **N1**, in contrast to **N2** and **N3**, which are composed of two different basic building blocks and will contain a statistically random combination of each. Due to the insolubility of the networks we could not form films for study by STM or AFM as has been recently done for sheets of a similar network made by Schlüter *et al.*[31] High resolution TEM images were obtained from deposits of **N1**

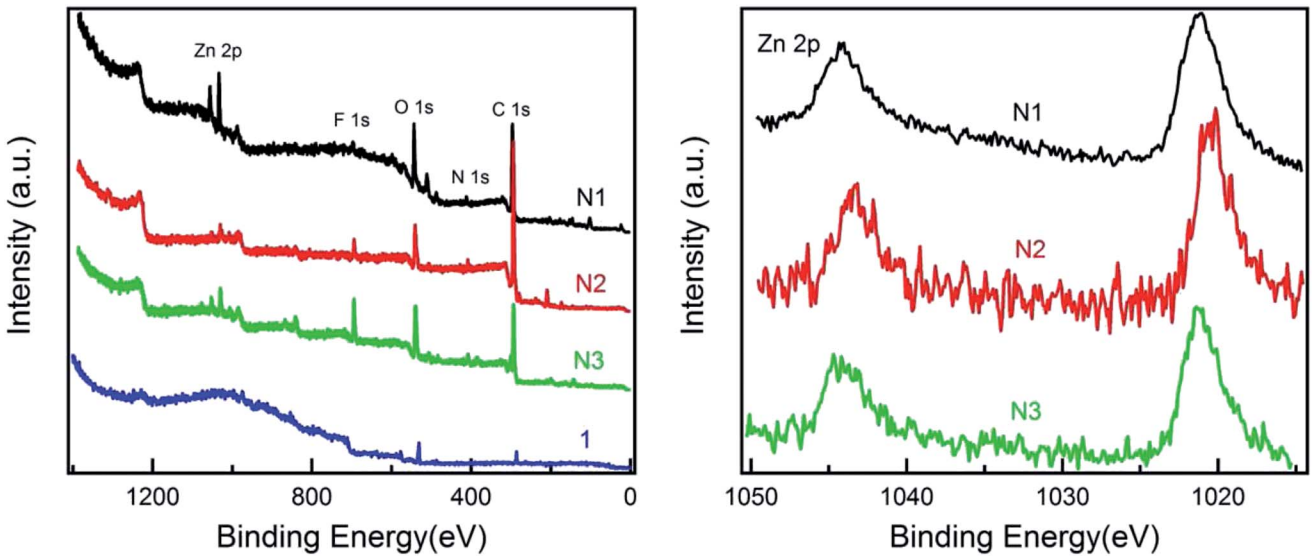

Fig. 2 XPS spectra of **1** and its zinc complexes **N1**, **N2** and **N3** on a carbon tape. Wide-scan spectra and zinc 2p region.

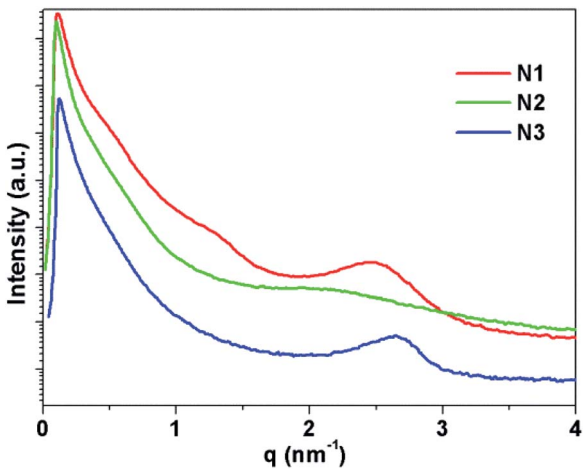

Fig. 3 Powder SAXS diffractogram of 2D networks **N1–3**.

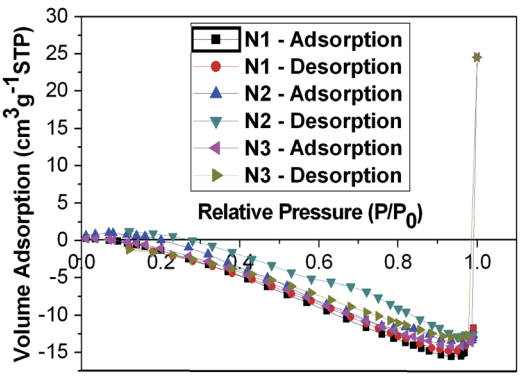

Fig. 4 Nitrogen adsorption–desorption isotherms of 2D networks **N1–3** measured at 77.3 K.

(see ESI†) on carbon coated copper grids but were unable to determine any structural data on the networks from them. Even with the use of electron energy loss spectroscopy (EELS) we were unable to see any peaks corresponding to the presence of zinc ions, which we attribute to the low concentration of the zinc in these networks.

Porosity studies

The porosity and the surface area of the 2D Zn^{2+} co-ordinated self-assembled networks **N1–3** were investigated by sorption analysis using nitrogen. The results are shown in Fig. 4 and summarized in Table S1 in the ESI.† In comparison to the covalently bonded organic microporous networks based on tetraphenylmethane reported earlier,[32–35] the surface areas of these networks are basically small (<2.1 $m^2\ g^{-1}$). All the values are well within the experimental error of the equipment. The negative dip for these networks is believed to be due to small sample size. These materials are thus believed to be highly interpenetrating networks, and hence no porosity was found, in these 2D Zn^{2+} co-ordinated self-assembled networks. Similar results were reported[12] for the 3D zinc metal ion co-ordinated networks with similar tpy branching units previously made by us. Shortening or removal of the long side chains is anticipated to solve this problem.

Structural modelling of 2D self-assembled networks

Atomistic models for network materials have previously shown that the node-strut topology is highly influential on the resulting structural properties of the network and their ability to pack to fill space efficiently.[32,33,36] Increased flexibility and conformational freedom of the network building blocks allow the networks to interpenetrate more freely and hence pack to fill more of the available space.[33,36a]

Firstly, atomistic models of the building blocks, **1** and **3**, and their respective one-component and two-component extended 3D self-assembled networks were generated. Models of **1** and **3**

were fully optimised using the COMPASS force field[37] in the *Forcite* module of Materials Studio 5.0 (ref. 38) with charges calculated using the Gasteiger method[39] and are shown in Fig. 5. Assessing the optimised geometry of model of **1** shows that the structure deviates from the idealised planar form. There are three angles that can be defined between the centroid of the central phenyl and the central nitrogen atom of two of the tpy ligands for **1**. These range between 103° and 138° compared to the ideal of 120°, and is 2 Å out of plane. The geometry of the optimised model for **3** shows a planar rigid molecule with the tpy-N–centroid–tpy-N angle being 177°.

Using these idealised building units, we have rationalised the SAXS data discussed above. For **N1**, there are four distinct repeat units available. These are, in order of dimension, (i) the

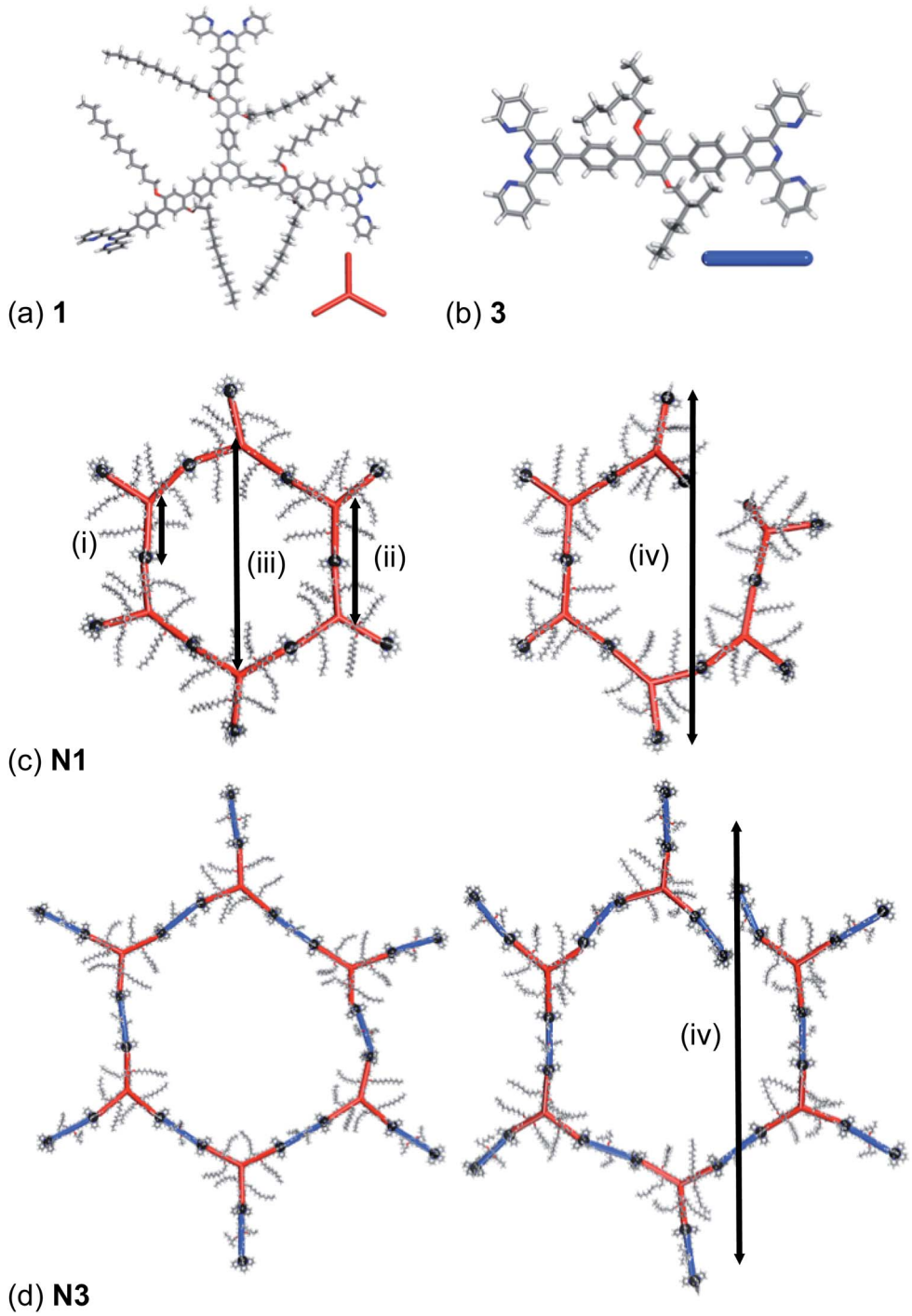

Fig. 5 The optimised geometry of (a) **1** and (b) **3** and idealised hexagons and broken hexagons for (c) **N1** and (d) **N3** respectively showing the four types of repeating distances potentially present within the extended network. The red rod inset in (a) represents **1** in the extended networks. The blue rod represents **3** in **N3**. The black spheres represent the linking Zn^{2+}.

distance between the molecular centroid of **1** and a coordinated Zn^{2+}, (ii) the molecular centroid – molecular centroid, and finally, depending upon the topology of the network either (iii) the molecular centroid – molecular centroid across a hexagonal repeat unit, if the network has a 2D graphite-like honeycomb structure, or (iv) a Zn^{2+} to opposite Zn^{2+} across a partial hexagonal ring, if the structure has a 3D structure. For **N3**, the two-component self-assembly results in a number of types of repeat units being available. These are the based on the same repeat units as identified for **N1**, but for each distinct repeat unit of **N1**, there are now a number of different combinations available for **N3**, particularly for repeat unit type (iii) where there will be multiple combinations possible. This variation in the build units results in the likelihood that these types will not be observed in SAXS measurements with only the build units of type (i) now being regular repeat units. These repeat units are identified in Fig. 5(c) and (d) for network **N1** and **N3** respectively.

A hexagonal and partial hexagon ring for both networks were generated for **N1** and **N3**, shown in Fig. 5(c) and (d) for network **N1** and **N3** respectively and were fully optimised using the COMPASS force field[37] in the *Forcite* module of Materials Studio 5.0 (ref. 38) with charges calculated using the Gasteiger method.[39] For **N1**, the average distance between repeat units (i) and (ii) is 2.0 nm and 4.0 nm respectively, correlating well to the observed peaks which have corresponding distances centred on 2.5 nm and 5.0 nm. For the idealised hexagon ring the type (iii) distance is 8.0 nm, which does not correlate well with the final peak observed in the SAXS data centred at 12.6 nm. For the partial hexagon ring, the type (iii) distance is 12.0 nm, which correlates well with the final peak observed in the SAXS diffractogram centred at 12.6 nm. This suggests that hexagon rings are not a significant structural component of **N1**. For **N3**, the type (i) average distances measure 2.0 nm (same as for **N1**) and 2.4 nm, which correspond well with the peak centred at a distance of 2.3 nm. No further peaks are observed in the SAXS diffractogram for **N3**, suggesting that the structural components of type (ii), (iii) or (iv) and are not repeating in dimension. This also suggests that hexagon ring formation is not a significant structural component of **N3**. The lack of a hexagon ring component in both **N1** and **N3** further suggests that the building blocks, **1** and **3** are not rigid structurally-directing units but have some conformational flexibility.

To fully explore the conformational freedom of the two building blocks, we have used molecular dynamic simulation at 100 K and 298 K using the *Forcite* module, the COMPASS force field and charges assigned using the Gasteiger method and with an NPT ensemble. For each simulation, a total of 2 ns simulation time with a 1.0 fs time step was used. The angles and out-of-plane distance are monitored for the final 1 ns of each simulation for **1** and **3**. For **1**, the three angles range between 64° and 174°. One angle and the out-of-plane distance is monitored throughout the 298 K MD simulation showing an average angle of $111 \pm 18°$ and an average out-of-plane distance of 6.4 ± 1.2 Å. It is noticeable that during the 298 K MD simulation the extended side chains wrap inwards towards the centre of the molecule. For **3**, the tpy–centroid–tpy angle ranges between 158° and 180° through out-of plane and in-plane molecular bends with a distance of between 0 Å and 2 Å out of the molecular plane. This demonstrates the high degree of flexibility and conformational freedom available to both **1** and **3** network building blocks.

We then turned our attention to the automated generation of a 3D self-assembled network structure. The 3D self-assembled networks were broken into fragment building units; these are not necessarily chemically representative of the actual monomeric reactants but enable us to automate the building process. For **N1**, we used two basic building units, Fragments A and B, shown in Fig. S.11(a) and (c) respectively in ESI.† For Fragment A (based on **1**), a library of 21 different conformers is available. This includes the idealised optimised structure and an additional 20 structures generated by sampling the two MD simulations. The MD simulations were sampled every 100 000 steps and the geometry of the resulting structures were optimised before the tpy end groups were removed. The remaining three unsaturated carbon atoms of the terminal phenyl groups were assigned as bonding atoms. The distance between the bonding atoms and the molecular centroid is approximately 14.0 Å. Fragment B is generated from the Zn^{2+} and the tpy coordinating ligands with the two PF_6^- counter ions. The geometry of both the Zn^{2+}-tpy and PF_6^- were fully optimised with DFT, using NWChem 6.1,[40] a def2-tzvp basis set,[41] B3LYP functional[42] and incorporating the Grimme dispersion correction.[43] A hydrogen atom is removed from the two central rings of each tpy group and the remaining unsaturated carbons were allocated as bonding atoms. The bonding atom – bonding atom distance is 9.7 Å. The incorporation of two PF_6^- groups within Fragment C ensures that these counter ions are accounted for within the network generation process. For **N3**, constructed from **1** and **3**, we included an additional Fragment C (shown in Fig. S.11(b) in ESI†), which is generated from a library of 5 conformers which include the idealised structure and an additional four created by sampling the MD simulation of **3**, similarly to **1**. The terminal tpy groups were removed and the remaining unsaturated carbons on the terminal phenyl groups are allocated as bonding atoms. The distance between the bonding atoms of Fragment C is 11.5 Å. Representative structures for Fragments A, B, and C are shown in Fig. S.11(c)–(e)† respectively with the bonding atoms highlighted in yellow. For Fragments A and C, Fig. S.11 and S.12† shows an overlay of the library of structures available for each fragment.

A Python code was used to automate the generation of the self-assembled network. The code builds the network following pre-set rules for a series of building steps. The first step is a *Seed* step where one or more fragments are added to a simulation cell of pre-set dimensions. We assign rules as to which Fragments are permitted to bond as follows; for network **N1**, Fragment A can bond to Fragment B, but not A to A or B to B, similarly for network **N3**. Fragment A can bond to B but not A or C and Fragment C can bond to B but not C or A. A *Build* step bonds a randomly selected additional fragment to a randomly selected existing fragment or partially built network. The fragment is bonded with idealised bond lengths, although the torsional angles of the fragments about the bond are random. Additional

bonds between fragments are only permitted if the bond geometry fits within the specified geometrical parameters, the bond distance is within a set range and no non-bonding atoms are closer than 1 Å. This ensures that the initial generation of the network is geometrically sensible.

We generated an idealised cluster for each network **N1** and **N3**. This enables us to assess the presence of the idealised structural components and their respective dimensions within an extended structure. The idealised clusters are generated exclusively from the idealised models of **1** and **3**, and do not include any of the structures obtained from the MD simulation. The idealised cluster for **N3** was generated following the idealised alternating **1** and **3** building pattern. The clusters were generated by an initial *Seed* step with one randomly chosen fragment and then a series of *Build* steps following the bonding rules. Each cluster Fragment is capped with either an uncoordinated tpy or a H atom. After generation, the geometry of the cluster is optimised using the Fast Inertial Relaxation Engine (FIRE) rigid body minimiser within HOOMD-blue.[44] The fragment build units are treated as rigid bodies so that only the bonds between fragments are optimised. The Intermolecular forces, bond and angle parameters are taken from the PCFF force field.[45] Intermolecular forces are described using a Lennard-Jones potential with additional Zn^{2+} parameters.[46] Charges are calculated using the Gasteiger method and QEq for the Zn^{2+} coordinated molecule in fragment B.[39] The idealised clusters for **N1** and **N3** are shown in Fig. S.12(a) and (b)† respectively. There are structural features of type (iv), as described above, present in both idealised networks **N1** and **N3**. For **N1**, the average is 11 nm and range between 10.0 nm and 14.4 nm, in good agreement with the range observed in the SAXs diffractogram for the peak centred at 12.6 nm with a range between 9 nm and 15.7 nm. For **N3**, the average is 16 nm and range between 19 nm and 14 nm. This does not correlate with any peaks in the diffractogram for **N3**. There are no structural components of type (iii) due to the automated network generation method. For **N1**, the type (i) and type (ii) are similar to the values obtained for the hexagon ring and for the partial ring. For the cluster model of idealised **N3**, the repeating structural components of type (ii) are well defined at 5.0 nm. We would expect to see peaks that correspond to both these distances in the SAXS diffractogram. These peaks are not present, with only peaks corresponding to the type (i) structural components present. This suggests that the regular alternating building unit model for **N3** does not represent the real structure. An alternative model for **N3** can be generated based on a randomised combination of the building block Fragments A and C.

Finally, we have constructed cluster models that include the structural flexibility observed in the MD simulations and randomised combination for **N3**. For **N1** and **N3** we have included the full library of structures for Fragment A and C. For network **N3** the choice is random between Fragment A and C with an equal probability for either Fragment. A representative cluster is shown in Fig. 6(a) and (b) for **N1** and **N3** respectively also showing the underlying net and fragment combination. Five clusters were generated for each network and are shown in Fig. S.13.† The clusters of network **N3** are largely planar, as might be expected from the two dimensionality of Fragment C, whereas those of **N1** extend in all three dimensions. We see a wide range of different combinations of Fragment A and C leading to a very wide range of structural components. The only repeat units observed in the randomised clusters of **N3** are those of type (i). This accounts for the absence of any peaks observed that do not correlate to type (i) distances within the SAXS diffractogram. Each cluster shows an extended structure with no evidence of order. The networks often turn in on

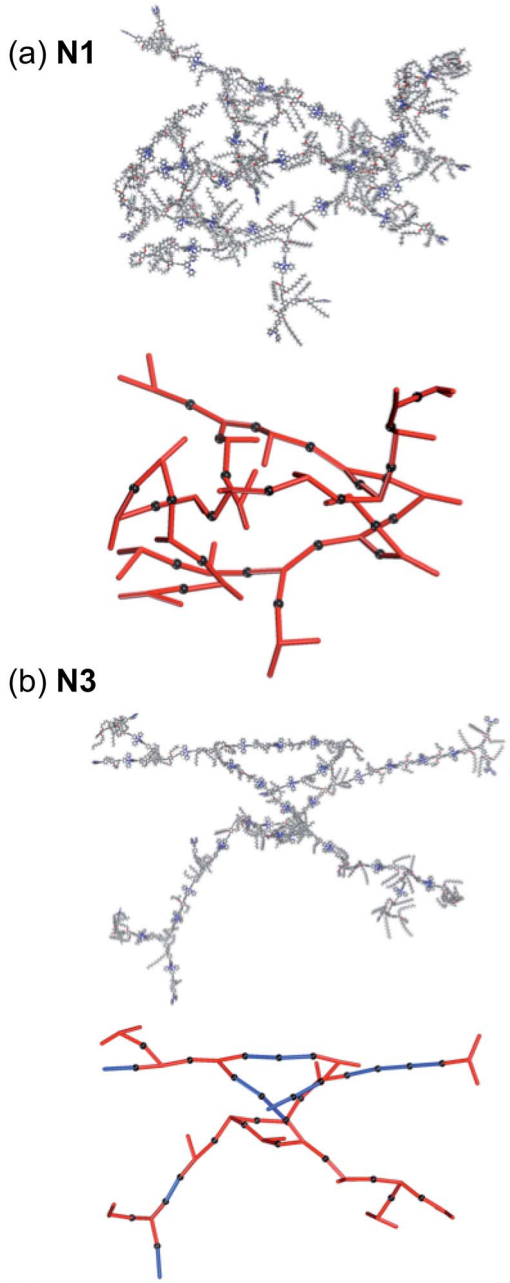

Fig. 6 Extended networks of (a) **N1** and (b) **N3** generated through an automated method with random choice of building block. Right – the network showing all atoms and, left – the underlying network with **1** and **3** represented as red and blue rods respectively. The black spheres represent the linking Zn^{2+}. The PF_6^- counter ions are omitted for clarity.

Table 1 5% weight loss temperature (T_{5d}), glass transition temperature (T_g) and melting temperature (T_m) of **1** and 2D networks **N1–3**

Networks	T_{5d}[a] (°C)	T_g[b] (°C)	T_m[c] (°C)
1	310	115	—[d]
N1	374	—[d]	—[d]
N2	390	—[d]	—[d]
N3	386	—[d]	—[d]

[a] T_{5d} = 5% weight loss temperature. [b] T_g = glass transition temperature. [c] T_m = melting temperature. [d] Relevant data is not found.

themselves, suggesting that network interpenetration is likely. This suggests that an amorphous, efficiently packed solid will be formed with no porosity. This is in agreement with the porosity study discussed above.

Thermal behaviour of 2D self-assembled networks

Thermogravimetric analysis (TGA) plots and Differential Scanning Calorimetry (DSC) plots of core molecule **1** and its 2D networks **N1–3** are shown in the ESI.† T_{5d}, T_g and T_m of 2D networks **N1–3** are listed in Table 1. According to Table 1, 2D zinc metal ion co-ordinated self-assembled networks **N1–3** have slightly higher T_{5d} compared to their respective starting materials **1**. Besides that, **N1–3** are generally more thermally stable compared to **1** as more than 50% of materials of **N1–3** remain after heating to 900 °C. Thus, Zn^{2+} co-ordination helped to improve the thermal stabilities of these Zn^{2+} co-ordinated networks **N1–3**. But no phase transitions (T_g and T_m) were observed in the DSC measurements of **N1–3**. Also, these 2D Zn^{2+} co-ordinated self-assembled networks **N1–3** are not crystalline as no significant exothermic peaks (T_c) have been observed during the heating cycles in their DSC plots.

Comparison of optical properties of 2D and 3D self-assembled networks

Photophysical properties of 2D self-assembled networks **N1–3** are in agreement with the observations for the terpyridine ligands and their 3D Zn^{2+} complexes discussed previously. Fig. 7(a) and (b) shows the appearance of self-assembled networks with naked eyes and under UV lamp respectively. The presence of Zn^{2+} ions in the molecular structure of the

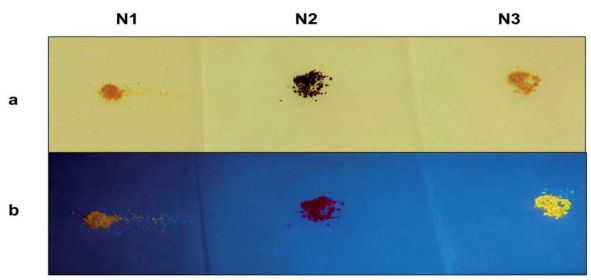

Fig. 7 (a) Solid appearance and (b) solid fluorescence of 2D networks **N1–3**.

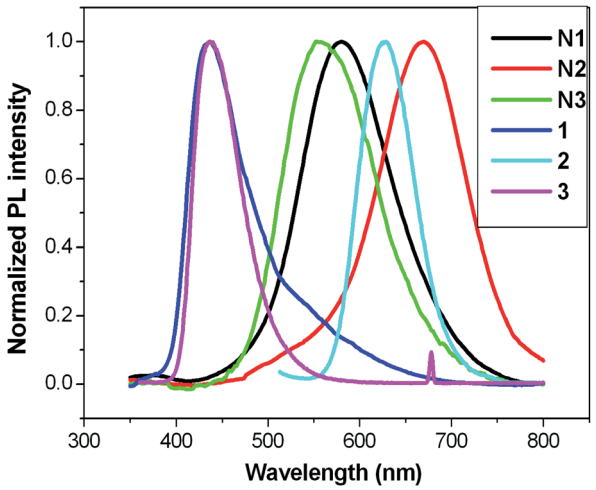

Fig. 8 Solid state photoluminescence spectra of core molecules **1**, **2**, **3** and their 2D self-assembled networks **N1–3**.

synthesized co-ordination networks **N1–3** is clearly indicated by the observed red shifts in the recorded emission spectra as shown in Fig. 8. Furthermore, the emission spectra of the discussed systems (**N1–3**) were measured in solid state at room temperature. Molecules **1**, **2** and **3** were emissive and the resulting Zn^{2+} co-ordination networks **N1–3** were emissive too. The solid state optical properties of the networks can be adjusted by inserting different types of linkers into the extended networks. This aspect might be explained by the fact that the synthesized metallo-supramolecular networks tend to aggregate mainly due to the conjugated and rigid structure of the spacers (**2** and **3**) and as well as core molecule **1**. Fig. 8 shows the emission spectra of core molecule **1** (emission peak at 436 nm) compared to the Zn^{2+} co-ordination networks **N1–3** demonstrating the red shift of 82, 233, and 115 nm respectively. **N2** shows red fluorescence under a UV lamp, as shown in Fig. 7, in comparison to the networks **N1** and **N3** both of which show yellow fluorescence under a UV lamp. This again shows the effect of the inserted n-type linker **2** which has a lower band gap and acts as sole emissive unit to produce red fluorescence in network **N2**, whereas, network **N3** which has the p-type linker **3** shows similar emission to network **N1**. Hence it is apparent that after Zn^{2+} ion complexation with tpy ligands, the position of the emission peak changes significantly.

Moreover, it was expected that the Zn^{2+} tpy connectivity will increase the electron delocalization on the conjugated and rigid spacers, which can be observed by red shift in the PL spectra of **N1–3**. The reason behind the red shift in the emission spectrum is the increase in conjugation, which will increase the number of delocalized electrons in the system. Finally, the longer the value of conjugation length, the lower will be the energy gap between closest energy levels and the longer will be the absorption wavelength, and so the emission wavelength too. Femtosecond time-resolved photoluminescence dynamics of **1** and its self-assembled networks **N1–3** and comparison with previously reported 3D networks has been performed. Fundamentally, fluorescence is a property of electronically excited

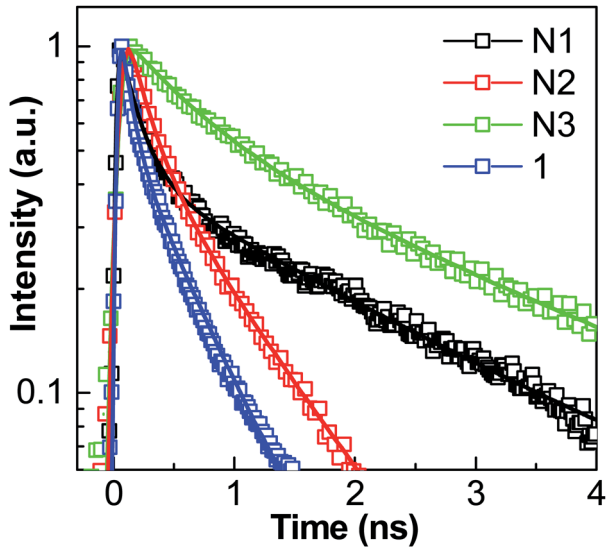

Fig. 9 Time-resolved fluorescence decay of **1** and its self-assembled networks **N1–3** in solid state.

Table 2 Lifetimes and pre-exponential factors from the fitting[a]

Networks	A_1	τ_1 (ns)	A_2	τ_1 (ns)	$\tau_{average}$ (ns)
1	0.56	0.10 ± 0.01	0.44	0.53 ± 0.02	0.45 ± 0.06
N1	0.63	0.17 ± 0.01	0.37	2.16 ± 0.02	1.92 ± 0.07
N2	0.60	0.19 ± 0.01	0.40	0.84 ± 0.01	0.68 ± 0.04
N3	0.46	0.61 ± 0.01	0.54	2.75 ± 0.02	2.41 ± 0.06

[a] An average lifetime, τ_a, was also calculated using $\tau_a = (A_1\tau_1^2 + A_2\tau_2^2)/(A_1\tau_1 + A_2\tau_2)$ for comparison.

states. Thus, fluorescence mechanisms can be better understood by time-resolved fluorescence spectroscopy. To obtain the dynamics of the PL spectra, the fluorescence lifetimes of compound **1** and its Zn^{2+} self-assembled networks **N1–3** were measured. The fluorescence decay behavior in the presence of Zn^{2+} is shown in Fig. 9, with the exponential fit results. Table 2 shows the fitted lifetimes and the pre-exponential factors. For comparison, we have also calculated the average lifetime. Comparatively, molecule **1** was found to show a shorter lifetime compared to **N1**, **N2** and **N3**. An increase in the fluorescence lifetime of networks **N1–3** was observed after zinc meal ion co-ordination of trigonal and linear terpyridine moiety in **1**, **2** and **3**. Similar results were observed of networks **S1** (similar to **N1**), **S3** (similar to **N3**) and **S4** (similar to **N2**) made up of a tetragonal tpy molecule (having similar branching units to trigonal tpy molecule **1**) previously reported by us (see ESI†).[12] The values of fluorescent life times are given in Table S1 in the ESI.† These results further suggest that networks with similar units have similar lifetime values. Enhancement in the lifetime after zinc metal ion co-ordination may be attributed to the increase in conjugation after metal complexation as observed with a red shift in the PL spectra too. These results also suggest a complete modification in the energy levels after zinc metal ion complexation. Networks **N2** and **S4** were formed by the n-type linker unit **2**, which has a lower band gap. Hence the fluorescence lifetime of these networks are also lower compared to the results obtained for **N1**, **S1**, **N3** and **S3** which were formed by the p-type linker units.

Experimental

Palladium tetrakis (triphenylphosphine) $Pd(PPh_3)_4$ was purchased from Strem Chemicals. Other reagents and solvents were purchased from Alfa Aesar and Fisher Scientific and were used as received. All reactions were carried out under an inert N_2 atmosphere. Analytical thin layer chromatography (TLC) was performed on aluminum sheets pre-coated with silica gel (with fluorescent indicator 254 nm). Visualization was accomplished with UV light. Purification of reaction mixtures using column chromatography was done on silica gel 60 Geduran (Merck). Nuclear magnetic resonance (NMR) spectra (^1H and ^{13}C) were recorded on a Bruker Advance 400 spectrometer, using magnetic field 400 MHz. Common solvents used in the NMR characterization were deuterated chloroform ($CDCl_3$) and DCM (CD_2Cl_2) and. Coupling constants (J) are reported as Hertz (Hz). NMR splitting patterns are designated as s, singlet; d, doublet; dd doublet of doublets, t, triplet; and m, multiplet. Mass spectra were recorded using a Shimadzu Axima Matrix-assisted laser desorption/ionization time-of-flight (MALDI-TOF) mass spectrometer. Thermogravimetric analysis (TGA) experiments were performed on a TA TGA-Q500 with a dynamic heat rate (10 °C min^{-1}) under nitrogen atmosphere (50 mL min^{-1}) in the temperature range 25–800 °C. Differential scanning calorimetry (DSC) measurements were performed on a TA DSC-Q10 with dynamic heating and cooling rate (5 °C min^{-1}) under nitrogen atmosphere (50 mL min^{-1}) in the temperature range 0–200 °C.

Synthesis of 1,3,5-tris(4-iodophenyl)benzene (4)

Compound **4** was synthesized as reported previously.[47]

Synthesis of triboronate (5)

4 (684.09 mg, 1 mmol), bis(pinacolato)diborane (1.15 g, 4.5 mmol), potassium acetate (1.18 g, 12 mmol) and $PdCl_2$(dppf) (65.85 mg, 0.09 mmol) were dissolved in anhydrous DMSO (15 mL) and then the solution was degassed under N_2 atmosphere. The resulting solution was stirred at 80 °C for 12 h, cooled to RT, and then poured into ice water. The extraction of the resulting reaction solution was done with $CHCl_3$ and water. Finally the $CHCl_3$ layers were dried over anhydrous $MgSO_4$. The solvent was evaporated with rotary evaporator; the residue was washed with cold hexane. Then the product was purified by recrystallization from MeOH–THF to afford **5** as an off-white solid (350 mg, 51%). ^1H NMR (400 MHz, $CDCl_3$): δ 7.93 (d, J = 8.2 Hz, 2H), 7.82 (s, 1H), 7.71 (d, J = 8.2 Hz, 2H), 1.37 (s, 12H).

Synthesis of intermediates 6, 7 and 8

2,5-Dibromobenzene-1,4-diol (2,5-dibromohydroquinone) was dialkylated to form 1,4-dibromo-2,5-bis(dodecyloxy)benzene **6**.[48] 4′-(4-Bromophenyl)-2,2′:6′2″-terpyridine **7** was synthesized through the reaction of 4-bromobenzaldehyde and

2-acetylpyridine.[49] The enolate of 2-acetylpyridine was produced by KOH under mild conditions, followed by an aldol condensation and a Michael addition. The intermediate, soluble diketone, was then permitted to form the central pyridine ring with an aqueous ammonia nitrogen source. Finally by boronation through a Miyaura reaction[50] **7** was converted to 4′-(4-pinacolatoboronphenyl)-2,2′:6′,2″-terpyridine **8**.

Synthesis of linear tpy compound (9)

6 (10 g, 16 mmol), **8** (4.0 g, 9.20 mmol), and $Pd(PPh_3)_4$ (638 mg, 0.55 mmol) were degassed using N_2 in a RBF. Degassed, THF (90 mL) and aqueous K_2CO_3 (2 M, 30 mL) were then injected into the RBF. The reaction mixture was then stirred in the dark at 80 °C for 24 h. After completion of the reaction (monitoring with TLC), the reaction mixture was cooled to RT and THF was removed using a rotary evaporator. The reaction mixture was then extracted with CH_2Cl_2. Organic layer was dried over $MgSO_4$; solvent was removed by rotary evaporator. Finally the compound was purified by column chromatography on alumina eluting with 10% EA in hexane. The product **9** was obtained as a off-white solid (4 g, 53%). ^{1}H NMR (400 MHz, $CDCl_3$): δ 8.98 (s, 1H), 8.77 (t, J = 8.0 Hz, 2H), 8.03–7.94 (m, 2H), 7.69 (d, J = 8.0 Hz, 1H), 7.41 (t, J = 6.0 Hz, 1H), 4.03 (t, J = 6.0 Hz, 1H), 3.900 (t, J = 6.0 Hz, 1H), 1.84 (t, J = 8 Hz, 1H), 1.71 (t, J = 8 Hz, 1H), 1.51 (t, J = 8 Hz, 1H), 1.26–1.19 (br, 16H), 0.89–0.81 (m, 3H). Anal. calcd for $C_{51}H_{66}BrN_3O_2$: C, 73.54; H, 7.99; Br, 9.59; N, 5.04; O, 3.84%. Found: C, 73.80; H, 10.63; N, 4.97%. HR ES$^+$-TOF MS: calculated m/z: 832.4417 (M^+), found: m/z 832.4398 (M^+).

Synthesis of trigonal tpy compound (1)

5 (0.10 mmol, 68 mg), **9** (0.6 mmol, 500 mg) and $Pd(PPh_3)_4$ (0.010 mmol, 12 mg) were put into RBF and degassed using N_2. Aqueous K_2CO_3 (2 M, 20 mL) and toluene (35 mL) were degassed using N_2 and then injected into the RBF. The reaction mixture was then stirred in the dark at 90 °C for 72 h and monitored by TLC. The reaction mixture was cooled to RT and toluene was removed using a rotary evaporator. The resulting reaction solution was then extracted with $CHCl_3$ and dried over $MgSO_4$. Solvent was removed with rotary evaporator and the pure compound was obtained by column chromatography on alumina eluting with 25% EA in hexane. **1** was obtained as an off-white solid (90 mg, 35%). ^{1}H NMR (400 MHz, CD_2Cl_2): δ 8.85 (s, 1H), 8.73 (dd, J = 11.4, 6.1 Hz, 2H), 8.05–7.72 (m, 12H), 7.70–7.48 (m, 1H), 7.46–7.32 (m, 3H), 7.17–7.09 (m, 2H), 4.02 (d, J = 5.8 Hz, 2H), 1.75 (s, 2H), 1.42 (s, 2H), 1.24 (d, J = 23.0 Hz, 16H), 0.84–0.80 (m, 3H). ^{13}C NMR (101 MHz, CD_2Cl_2): δ 156.76, 156.64, 151.04, 149.77, 130.79, 130.69, 130.60, 128.38, 128.04, 127.45, 127.35, 124.47, 121.71, 119.10, 116.62, 116.46, 70.27, 54.00, 35.21, 32.49, 32.17, 30.23, 30.21, 29.93, 26.75, 25.82, 23.23, 14.45, 11.76. HR ES$^+$-TOF MS: calculated m/z: 2562.6750 (M^+), found: m/z 2562.6750 (M^+).

Synthesis of Zn^{2+}-self-assembled network of 1 (N1)

To a solution of **1** (25 mg, 0.010 mmol) in NMP (10 mL), zinc(II) acetate dihydrate (4.2 mg, 0.015 mmol) in NMP (2 mL) was added dropwise. The resulting solution was then stirred at 105 °C under N_2 atmosphere for 24 h. An excess of NH_4PF_6 was then added into the hot solution and stirring was continued for 30 min. The resulting reaction solution was added slowly into MeOH for precipitation. The precipitate was then filtered off and washed with MeOH. The precipitate was again dissolved in NMP followed by reprecipitation of the solid by adding ether. The precipitate was dried under vacuum for 24 h to give **N1** as a yellow solid (27 mg, 74%).

Synthesis of Zn^{2+} self-assembled network of 1 with 2 (N2)

N1 (15 mg, 0.005 mmol) in NMP (10 mL) was heated to 105 °C. Zn^{2+} acetate dihydrate (2.18 mg, 0.008 mmol) in NMP (2 mL) was added dropwise into the resulting solution. The reaction mixture was stirred at 105 °C under N_2 for 1 h. **2** (9.63 mg, 0.0075 mmol, 1.5 times **N1** moles) in NMP (10 mL) was then added dropwise and the resulting reaction mixture was stirred at 105 °C under N_2 for 24 h. An excess of NH_4PF_6 was then added into the hot reaction mixture and stirring was continued for 30 min. The resulting reaction solution was added slowly into MeOH for precipitation. The precipitate was then filtered off and washed with MeOH. The precipitate was again dissolved in NMP followed by reprecipitation of the solid by adding ether. The precipitate was dried under vacuum for 24 h to give **N2** as a red solid (14 mg, 62%).

Synthesis of Zn^{2+}-self-assembled network of 1 with 3 (N3)

N1 (15 mg, 0.005 mmol) in NMP (10 mL) was heated to 105 °C. Zn^{2+} acetate dihydrate (2.2 mg, 0.0075 mmol) in NMP (2 mL) was added dropwise into the reaction mixture. The reaction mixture was stirred at 105 °C under N_2 for 1 h. **3** (7.2 mg, 0.0075 mmol, 1.5 times **N1** moles) in NMP (10 mL) was then added dropwise and the resulting reaction mixture was stirred at 105 °C under N_2 for 24 h. An excess of NH_4PF_6 was then added into the hot reaction mixture and stirring was continued for 30 min. The resulting reaction solution was added slowly into MeOH for precipitation. The precipitate was then filtered off and washed with MeOH. Precipitate was again dissolved in NMP followed by reprecipitation of the solid by adding ether. The precipitate was dried under vacuum for 24 h to give **N3** as a yellow solid (12 mg, 55%).

Spectroscopic characterizations

For the measurements of photoluminescence (PL) spectra, a cw He–Cd laser emitting at 325 nm was used as the excitation source and the signals were dispersed by a 750 mm monochromator combined with suitable filters, and detected by a photomultiplier using the standard lock-in amplifier technique. Time-resolved photoluminescence (TRPL) spectroscopy was performed using 325 nm laser pulses generated from an optical parametric amplifier parametric amplifier (Light Conversion TOPAS) that was pumped by a 1 kHz regenerative amplifier (Coherent Legend; center wavelength: 800 nm; pulse width: 150 fs; power: 1 mJ per pulse), which was in turn seeded by an 80 MHz Coherent Vitesse oscillator. The TRPL signals were collected in a typical backscattering geometry by a pair of lenses to a DK240 1/4 m monochromator with 300 g mm^{-1} grating,

and the temporal evolution of the PL was resolved by an Optronis Optoscope streak camera system. The streak camera system has an ultimate temporal resolution of ~10 ps when operated at the shortest time window of 330 ps.

Conclusions

Synthesis and characterization of various Zn^{2+} terpyridine 2D self-assembled networks were described in this work. Their thermal and photophysical properties were studied in detail and compared to the constituent chelating terpyridine ligands. These 2D co-ordination networks are found to be thermally stable as compared to their starting materials, especially at very high temperature due to the effect of zinc metal ion co-ordination.

2D Zn^{2+} supramolecular networks were compared to the 3D Zn^{2+} networks in order to understand the influence of the Zn^{2+} ions on the photophysical properties of the designed structures. The synthesized 2D Zn^{2+} co-ordination networks revealed marked red shifts in the emission spectra like the 3D Zn^{2+} networks made up of similar building blocks. It was observed that the presence of the Zn^{2+} ions in the synthesized model complexes revealed interesting spectroscopic properties, in particular, enhanced fluorescence and fluorescence life time. Thus, from the experimental results it was concluded that the characteristics of the basic building units are considerably influencing the photophysical properties of the Zn^{2+} co-ordination networks. Such Zn^{2+} systems could be potentially interesting for the construction of optoelectronic devices.

Acknowledgements

We acknowledge the financial support, including the award of a Research Student Scholarship to D.R., from the Singapore Ministry of Education through the Academic Research Fund Tier 1 (SUG 40/06 and RG19/07) and also from the National Research Foundation through Competitive Research Project 5-2009-04 "Towards Efficient Sunlight Harvesting". A.T holds a Royal Society fellowship. We thank Dr Zviad Tsakadze and Miss Anantha P. from the School of Materials Science and Engineering, NTU for performing SAXS and TEM measurements respectively.

Notes and references

1 H. Hofmeier and U. S. Schubert, *Chem. Soc. Rev.*, 2004, **33**, 373.
2 S. Burattini, H. M. Colquhoun, J. D. Fox, D. Friedmann, B. W. Greenland, P. J. F. Harris, W. Hayes, M. E. Mackay and S. J. Rowan, *Chem. Commun.*, 2009, 6717.
3 F. Cacialli, P. Samorì and C. Silva, *Mater. Today*, 2004, **7**, 24–32.
4 S. De Feyter and F. C. De Schryver, *Chem. Soc. Rev.*, 2003, **32**, 139–150.
5 A. Langner, S. L. Tait, C. Rajadurai, M. Ruben and K. Kern, *Chem. Commun.*, 2007, 4860–4862.
6 T. Chen, G.-B. Pan, H. Wettach, M. Fritzsche, S. Höger, L.-J. Wan, H.-B. Yang, B. H. Northrop and P. J. Stang, *J. Am. Chem. Soc.*, 2010, **132**, 1328–1333.
7 R. Chakrabarty, P. S. Mukherjee and P. J. Stang, *Chem. Rev.*, 2011, **111**, 6810–6918.
8 T. Chen, G.-B. Pan, H. Wettach, M. Fritzsche, S. Höger, L.-J. Wan, H.-B. Yang, B. H. Northrop and P. J. Stang, *J. Am. Chem. Soc.*, 2010, **132**, 1328–1333.
9 O. Ivasenko, J. M. MacLeod, K. Y. Chernichenko, E. S. Balenkova, R. V. Shpanchenko, V. G. Nenajdenko, F. Rosei and D. F. Perepichka, *Chem. Commun.*, 2009, 1192.
10 M. Ruben, U. Ziener, J. M. Lehn, V. Ksenofontov, P. Gütlich and G. Vaughan, *Chem.–Eur. J.*, 2004, **11**, 94–100.
11 T. Bauer, A. Schlüter and J. Sakamoto, *Synlett*, 2010, 877–880.
12 Z. B. Lim, H. Li, S. Sun, J. Y. Lek, A. Trewin, Y. M. Lam and A. C. Grimsdale, *J. Mater. Chem.*, 2012, **22**, 6218.
13 Y. Ohba, K. Kanaizuka, M. Murata and H. Nishihara, *Macromol. Symp.*, 2006, **235**, 31–38.
14 L. J. Liang, X. J. Zhao and C. Z. Huang, *Analyst*, 2012, **137**, 953.
15 X. Zhou, X. Jin, D. Li and X. Wu, *Chem. Commun.*, 2011, **47**, 3921.
16 X. Chen, Q. Zhou, Y. Cheng, Y. Geng, D. Ma, Z. Xie and L. Wang, *J. Lumin.*, 2007, **126**, 81–90.
17 S.-H. Hwang, C. N. Moorefield, P. Wang, J.-Y. Kim, S.-W. Lee and G. R. Newkome, *Inorg. Chim. Acta*, 2007, **360**, 1780–1784.
18 A. Winter, C. Friebe, M. Chiper, M. D. Hager and U. S. Schubert, *J. Polym. Sci., Part A: Polym. Chem.*, 2009, **47**, 4083–4098.
19 T. He, D. Rajwar, L. Ma, Y. Wang, Z. B. Lim, A. C. Grimsdale and H. Sun, *Appl. Phys. Lett.*, 2012, **101**, 213302.
20 D. W. Fink and W. E. Ohnesorge, *J. Phys. Chem.*, 1970, **74**, 72–77.
21 U. S. Schubert, C. Eschbaumer, O. Hien and P. R. Andres, *Tetrahedron Lett.*, 2001, **42**, 4705–4707.
22 X. Yan, F. Wang, B. Zheng and F. Huang, *Chem. Soc. Rev.*, 2012, **41**, 6042–6065.
23 A. Wild, A. Winter, F. Schlütter and U. S. Schubert, *Chem. Soc. Rev.*, 2011, **40**, 1459–1511.
24 A. Wild, C. Friebe, A. Winter, M. D. Hager, U. W. Grummt and U. S. Schubert, *Eur. J. Org. Chem.*, 2010, **2010**, 1859–1868.
25 G. R. Newkome, *Science*, 2006, **312**, 1782–1785.
26 A. L. Kanibolotsky and P. J. Skabara, *Chem. Soc. Rev.*, 2010, **39**, 2695–2728.
27 V. Duprez, M. Biancardo, H. Spanggaard and F. C. Krebs, *Macromolecules*, 2005, **38**, 10436–10448.
28 C. J. Kuehl, S. D. Huang and P. J. Stang, *J. Am. Chem. Soc.*, 2001, **123**, 9634–9641.
29 B. H. Northrop, Y.-R. Zheng, K.-W. Chi and P. J. Stang, *Acc. Chem. Res.*, 2009, **42**, 1554–1563.
30 A. D'Aléo, E. Cecchetto, L. De Cola and R. M. Williams, *Sensors*, 2009, **9**, 3604–3626.
31 Z. Zheng, C. S. Ruiz-Vargas, T. Bauer, A. Rossi, P. Payamyar, A. Schütz, A. Stemmer, J. Sakamoto and A. D. Schlüter, *Macromol. Rapid Commun.*, 2013, **34**, 1670–1680.
32 J.-X. Jiang, F. Su, A. Trewin, C. D. Wood, N. L. Campbell, H. Niu, C. Dickinson, A. Y. Ganin, M. J. Rosseinsky,

Y. Z. Khimyak and A. I. Cooper, *Angew. Chem., Int. Ed.*, 2007, **46**, 8574–8578.
33 J.-X. Jiang, F. Su, A. Trewin, C. D. Wood, H. Niu, J. T. A. Jones, Y. Z. Khimyak and A. I. Cooper, *J. Am. Chem. Soc.*, 2008, **130**, 7710–7720.
34 T. Tozawa, J. T. A. Jones, S. I. Swamy, S. Jiang, D. J. Adams, S. Shakespeare, R. Clowes, D. Bradshaw, T. Hasell, S. Y. Chong, C. Tang, S. Thompson, J. Parker, A. Trewin, J. Bacsa, A. M. Z. Slawin, A. Steiner and A. I. Cooper, *Nat. Mater.*, 2009, **8**, 973–978.
35 Q. Chen, M. Luo, T. Wang, J.-X. Wang, D. Zhou, Y. Han, C.-S. Zhang, C.-G. Yan and B.-H. Han, *Macromolecules*, 2011, **44**, 5573–5577.
36 (*a*) J. Jiang, A. Trewin, F. Su, C. D. Wood, H. Niu, J. T. A. Jones, Y. Z. Khimyak and A. I. Cooper, *Macromolecules*, 2009, **42**, 2658–2666; (*b*) E. Stockel, X. Wu, A. Trewin, C. D. Wood, R. Clowes, N. L. Campbell, J. T. A Jones, Y. Z. Khimyak, D. J. Adams and A. I. Cooper, *Chem. Commun.*, 2009, 212–214.
37 H. Sun, *J. Phys. Chem. B*, 1998, **102**, 7338–7364.
38 Accelrys, *Materials Studio 5.0*, San Diego, CA, 2009.
39 J. Gasteiger and M. Marsill, *Tetrahedron*, 1990, **36**, 3219–3228.
40 M. Valiev, E. J. Bylaska, N. Govind, K. Kowalski, T. P. Straatsma, H. J. J. Van Dam, D. Wang, J. Nieplocha, E. Apra, T. L. Windus and W. A. de Jong, *Comput. Phys. Commun.*, 2010, **181**, 1477–1489.
41 F. Weigend and R. Ahlrichs, *Phys. Chem. Chem. Phys.*, 2005, **7**, 3297–3305.
42 (*a*) A. D. Becke, *J. Chem. Phys.*, 1993, **98**, 5648–5652; (*b*) C. Lee, W. Yang and R. G. Parr, *Phys. Rev. B: Condens. Matter Mater. Phys.*, 1988, **37**, 785.
43 S. Grimme, J. Antony, S. Ehrlich and H. Krieg, *J. Chem. Phys.*, 2010, **132**, 154104–154119.
44 (*a*) J. A. Anderson, C. D. Lorenz and A. Travesset, *J. Comput. Phys.*, 2008, **227**, 5342–5359; (*b*) T. D. Nguyen, C. L. Phillips, J. A. Anderson and S. C. Glotzer, *Comput. Phys. Commun.*, 2011, **182**, 2307–2313; (*c*) http://codeblue.umich.edu/hoomd-blue, HOOMD-blue web page.
45 (*a*) H. Sun, S. J. Mumby, J. R. Maple and A. T. Hagler, *J. Am. Chem. Soc.*, 1994, **116**, 2978–2987; (*b*) H. Sun, *Macromolecules*, 1995, **28**, 701–712; (*c*) H. Sun, *J. Comput. Chem.*, 1994, **15**, 752–768.
46 J. Torras and C. Aleman, *J. Phys. Chem. B*, 2013, **117**, 10513–10522.
47 S. Kotha, D. Kashinath, K. Lahiri and R. B. Sunoj, *Eur. J. Org. Chem.*, 2004, **2004**, 4003–4013.
48 C. Baskar, Y.-H. Lai and S. Valiyaveettil, *Macromolecules*, 2001, **34**, 6255–6260.
49 J. Wang and G. S. Hanan, *Synlett*, 2005, 1251–1254.
50 C. J. Aspley and J. A. Gareth Williams, *New J. Chem.*, 2001, **25**, 1136–1147.